How Abnormal Are the PDFs of the DIA Method
A Quality Description in the Context of GNSS

Zaminpardaz, Safoora; Teunissen, Peter J.G.

DOI
10.1007/1345_2019_57

Publication date
2019

Document Version
Final published version

Published in
9th Hotine-Marussi Symposium on Mathematical Geodesy - Proceedings of the Symposium in Rome, 2018

Citation (APA)
Zaminpardaz, S., & Teunissen, P. J. G. (2019). How Abnormal Are the PDFs of the DIA Method: A Quality Description in the Context of GNSS. In P. Novák, M. Crespi, N. Sneeuw, & F. Sansò (Eds.), *9th Hotine-Marussi Symposium on Mathematical Geodesy - Proceedings of the Symposium in Rome, 2018* (pp. 89-97). (International Association of Geodesy Symposia; Vol. 151). Springer.
https://doi.org/10.1007/1345_2019_57

How Abnormal Are the PDFs of the DIA Method: A Quality Description in the Context of GNSS

Safoora Zaminpardaz and Peter J. G. Teunissen

Abstract

The DIA-method, for the detection, identification and adaptation of modeling errors, has been widely used in a broad range of applications including the quality control of geodetic networks and the integrity monitoring of GNSS models. The DIA-method combines two key statistical inference tools, estimation and testing. Through the former, one seeks estimates of the parameters of interest, whereas through the latter, one validates these estimates and corrects them for biases that may be present. As a result of this intimate link between estimation and testing, the quality of the DIA outcome $\bar{x}$ must also be driven by the probabilistic characteristics of both estimation and testing. In practice however, the evaluation of the quality of $\bar{x}$ is never carried out as such. Instead, use is made of the probability density function (PDF) of the estimator under the identified hypothesis, say $\hat{x}_i$, thereby thus neglecting the conditioning process that led to the decision to accept the i^{th} hypothesis. In this contribution, we conduct a comparative study of the probabilistic properties of $\bar{x}$ and $\hat{x}_i$. Our analysis will be carried out in the framework of GNSS-based positioning. We will also elaborate on the circumstances under which the distribution of the estimator $\hat{x}_i$ provides either poor or reasonable approximations to that of the DIA-estimator $\bar{x}$.

Keywords

Detection, identification and adaptation (DIA) · DIA-estimator · Global Navigation Satellite System (GNSS) · Probability density function (PDF) · Statistical testing

1 Introduction

In the DIA-method for the detection, identification and adaptation of mismodelling errors, next to estimation of parameters of interest, a statistical testing is also exercised to check the validation of underlying model. The actual DIA outcome is then the one which rigorously captures this combination of estimation and testing, and was introduced as the *DIA estimator* in Teunissen (2017b). The DIA-method has been widely used in a variety of applications, including the quality control of geodetic networks and the integrity monitoring of GNSS models, see e.g. DGCC (1982), Teunissen (1990), Salzmann (1995), Tiberius (1998), Perfetti (2006), Khodabandeh and Teunissen (2016), Zaminpardaz et al. (2015). As a result of the combined estimation-testing scheme of the DIA-method, the DIA outcome $\bar{x}$ must also be evaluated on the basis of characteristics of both estimation and testing. In practice however, the evaluation of the quality of $\bar{x}$ is carried out based upon the probability density function (PDF) of the estimator under the identified hypothesis, say

S. Zaminpardaz (✉)
Geospatial Sciences, School of Science, RMIT University, Melbourne, VIC, Australia
e-mail: safoora.zaminpardaz@rmit.edu.au

P. J. G. Teunissen
Department of Geoscience and Remote Sensing, Delft University of Technology, Delft, The Netherlands

GNSS Research Centre, School of Earth and Planetary Sciences, Curtin University, Perth, WA, Australia
e-mail: p.j.g.teunissen@tudelft.nl

P. Novák et al. (eds.), *IX Hotine-Marussi Symposium on Mathematical Geodesy*,
International Association of Geodesy Symposia 151, https://doi.org/10.1007/1345_2019_57

$\hat{x}_i$, without regard to the conditioning process that led to the decision of accepting the hypothesis $\mathcal{H}_i$. In this contribution, a comparative study of the probabilistic properties of $\bar{x}$ and $\hat{x}_i$ is conducted to highlight the impact of neglecting the estimation-testing link on follow-on quality evaluations and to elaborate on the circumstances under which such negligence may still be considered acceptable.

This contribution is organized as follows. We first give a brief overview of the Detection, Identification, and Adaptation procedure in Sect. 2. Using a partitioning of the misclosure space, the DIA-estimator and its statistical distribution are then presented in Sect. 3. The difference between the PDF of the DIA-estimator and that of $\hat{x}_i$ is discussed and shown to be driven by the DIA-method decision probabilities which can be categorized as probability of correct acceptance (CA), of false alarm (FA), of correct/missed detection (CD/MD) and of correct/wrong identification (CI/WI). In Sect. 4, we outline the estimation and testing strategies that we use for our analyses. Section 5 contains our numerical evaluations of the distribution of the DIA-estimator $\bar{x}$ and its normally-distributed individual components $\hat{x}_i$ $(i = 0, 1, \ldots, k)$. We graphically demonstrate, for binary hypothesis testing, i.e. $\mathcal{H}_0$ and $\mathcal{H}_1$, applied to a single-unknown, single-redundancy observational model, the PDF of $\bar{x}$, $\hat{x}_0$ and $\hat{x}_1$ under both $\mathcal{H}_0$ and $\mathcal{H}_1$. The distributional comparison is then continued for a Global Navigation Satellite System (GNSS) single point positioning (SPP) model where multiple-hypothesis testing is involved. Finally a summary with conclusions are presented in Sect. 6.

2 DIA Overview

As our point of departure, we first formulate our statistical hypotheses. The hypothesis believed to be true under nominal working conditions is referred to as the *null hypothesis*. Denoted by $\mathcal{H}_0$, the null hypothesis is assumed to be given as

$$\mathcal{H}_0: \quad \mathsf{E}(y) = A\,x \quad , \quad \mathsf{D}(y) = Q_{yy} \tag{1}$$

with $\mathsf{E}(\cdot)$ and $\mathsf{D}(\cdot)$ denoting the expectation and dispersion operators, respectively. According to (1), under $\mathcal{H}_0$, the expectation of the normally-distributed random vector of observables $y \in \mathbb{R}^m$ is characterized through the unknown parameter vector $x \in \mathbb{R}^n$ and the full-rank design matrix $A \in \mathbb{R}^{m\times n}$ $(\text{rank}(A) = n)$, while the dispersion of the observables y is described by the positive-definite variance-covariance matrix $Q_{yy} \in \mathbb{R}^{m\times m}$. The redundancy of $\mathcal{H}_0$ is $r = m - \text{rank}(A) = m - n$. The corresponding estimator of x on the basis of (1) is denoted by $\hat{x}_0$.

The observational model in (1) could be misspecified in several ways like, for example, $\mathsf{E}(y) \neq A\,x$ and/or $\mathsf{D}(y) \neq Q_{yy}$. Here we assume that a misspecification is restricted to an underparametrization of the mean of y, which is the most common error that occurs when formulating the model (Teunissen 2017a). Thus, the alternative hypothesis $\mathcal{H}_i$ is formulated as

$$\mathcal{H}_i: \quad \mathsf{E}(y) = A\,x + C_i\,b_i \quad , \quad \mathsf{D}(y) = Q_{yy} \tag{2}$$

where $b_i \in \mathbb{R}^q$ is the unknown bias vector while $C_i \in \mathbb{R}^{m\times q}$ is known which together with the design matrix A form a full-rank matrix, i.e. $\text{rank}([A,\ C_i]) = n + q$ with $q \leq m - n$. The corresponding estimator of x on the basis of (2) is denoted by $\hat{x}_i$.

In practical applications, we usually have to consider several alternative hypotheses about the physical reality at hand. For example when modeling GNSS observations, we may need to take into account hypotheses describing code outliers, phase cycle slips, ionospheric gradients, etc. The statistical validity of $\mathcal{H}_0$ and the multiple, say k, alternatives $\mathcal{H}_i$ $(i = 1, \ldots, k)$ is usually checked through the following three steps of detection, identification and adaptation (DIA) (Baarda 1968; Teunissen 1990).

1. *Detection* The null hypothesis undergoes a validity check using an overall model test, without considering a particular set of alternatives. If $\mathcal{H}_0$ is accepted, then $\hat{x}_0$ is provided as the estimate of x.
2. *Identification* In case $\mathcal{H}_0$ is rejected, a search is carried out among the specified alternative hypotheses $\mathcal{H}_i$ $(i = 1, \ldots, k)$ with the purpose of pinpointing the potential source of model error. In doing so, one of the alternative hypotheses, say $\mathcal{H}_i$, is identified as the suspected model error.
3. *Adaptation* The identified hypothesis $\mathcal{H}_i$ becomes the new null hypothesis. The $\mathcal{H}_0$-based inferences are then accordingly corrected and $\hat{x}_i$ is provided as the estimate of x.

The required information to realize the above steps of the DIA-method is contained in the *misclosure* vector $t \in \mathbb{R}^r$ given as

$$t = B^T y; \qquad Q_{tt} = B^T Q_{yy} B \tag{3}$$

where $B \in \mathbb{R}^{m\times r}$ is a full-rank matrix, with $\text{rank}(B) = r$, such that $[A,\ B] \in \mathbb{R}^{m\times m}$ is invertible and $A^T B = 0$. With $y \overset{\mathcal{H}_i}{\sim} \mathcal{N}(Ax + C_i b_i, Q_{yy})$ for $i = 0, 1, \ldots, k$ and $C_0 b_0 = 0$, the misclosure vector is then distributed as

$$t \overset{\mathcal{H}_i}{\sim} \mathcal{N}(\mu_{t_i} = B^T C_i b_i, Q_{tt}), \qquad \text{for} \quad i = 0, 1, \ldots, k \tag{4}$$

An unambiguous testing procedure can be established through unambiguously assigning the outcomes of t to the

statistical hypotheses $\mathcal{H}_i$ for $i = 0, 1, \ldots, k$, which can be realized through a partitioning of the misclosure space (Teunissen 2017b). As such, let $\mathcal{P}_i \in \mathbb{R}^r$ $(i = 0, 1, \ldots, k)$ be a partitioning of the misclosure space $\mathbb{R}^r$, i.e. $\cup_{i=0}^{k} \mathcal{P}_i = \mathbb{R}^r$ and $\mathcal{P}_i \cap \mathcal{P}_j = \emptyset$ for $i \neq j$, then the unambiguous testing procedure is defined as follows (Teunissen 2017b)

$$\text{Select } \mathcal{H}_i \iff t \in \mathcal{P}_i, \qquad \text{for } i = 0, 1, \ldots, k \tag{5}$$

3 On the Outcome of the DIA Method

Looking at the three steps of the DIA-method presented in Sect. 2, it can be realized that estimation and testing are combined in the DIA procedure. To gain a better appreciation of this combination, the DIA procedure is schematically visualized in Fig. 1. One can then find out that this is indeed the testing decision which determines how to estimate the unknown parameter vector x. Therefore, the actual DIA outcome, denoted by $\bar{x}$, will inherit the characteristics of not only the estimation scheme but also the testing scheme as well.

3.1 DIA Estimator

The combined estimation-testing scheme of the DIA-method can be captured in one single *DIA estimator* which was introduced in Teunissen (2017b) and is formulated as

$$\bar{x} = \sum_{i=0}^{k} \hat{x}_i \, p_i(t) \tag{6}$$

in which the contribution to $\bar{x}$ from the estimation scheme is captured by the individual estimators $\hat{x}_i$ $(i = 0, 1, \ldots, k)$, and from the testing scheme by the indicator functions $p_i(t)$ $(i = 0, 1, \ldots, k)$ defined as $p_i(t) = 1$ if $t \in \mathcal{P}_i$ and $p_i(t) = 0$ elsewhere. The DIA outcome $\bar{x}$ is therefore a binary weighted average of all the solutions corresponding with the hypotheses at hand. We note that although $\bar{x}$ is linear in the estimators $\hat{x}_i$ $(i = 0, 1, \ldots, k)$, it is nonlinear in t as the indicator functions $p_i(t)$ $(i = 0, 1, \ldots, k)$ are nonlinear functions of t. As a consequence, even if all the individual estimators $\hat{x}_i$ $(i = 0, 1, \ldots, k)$ are normally distributed, $\bar{x}$ does *not* have a normal distribution.

3.2 Abnormality of the PDF of $\bar{x}$

A general probabilistic evaluation of the DIA-estimator is presented in Teunissen (2017b), see also Teunissen et al. (2017). With (6), the probability density function (PDF) of $\bar{x}$, under an arbitrary hypothesis like $\mathcal{H}_j$, can be expressed in terms of the probabilistic properties of the estimators $\hat{x}_i$ $(i = 0, 1, \ldots, k)$ and t as

$$f_{\bar{x}}(\theta|\mathcal{H}_j) = \sum_{i=0}^{k} \int_{\mathcal{P}_i} f_{\hat{x}_i,t}(\theta, \tau|\mathcal{H}_j) \, d\tau \tag{7}$$

where $f_{\hat{x}_i,t}(\theta, \tau|\mathcal{H}_j)$ is the joint PDF of $\hat{x}_i$ and t under $\mathcal{H}_j$. The abnormality of the DIA-estimator PDF can clearly be seen in the above equation. It is important to note, upon application of the DIA-method, that all the follow-on evaluations and inferences must be derived from the probabilistic properties of $\bar{x}$ which are captured by its PDF in (7). In practice however, if a certain hypothesis, say $\mathcal{H}_i$, is selected through the testing procedure, use is made of the PDF of the estimator under the selected hypothesis, i.e. $\hat{x}_i$, neglecting the conditioning process that led to the decision to accept this hypothesis, see e.g. Salzmann (1995), Klein et al. (2018).

To get a better insight into what such negligence could incur, we highlight the difference between the PDF of the DIA-estimator $\bar{x}$ and that of the estimator $\hat{x}_i$, which, under $\mathcal{H}_j$, can be expressed in

$$\begin{aligned} &f_{\bar{x}}(\theta|\mathcal{H}_j) - f_{\hat{x}_i}(\theta|\mathcal{H}_j) = \\ &\left\{ f_{\bar{x}|t\notin\mathcal{P}_i}(\theta|t \notin \mathcal{P}_i, \mathcal{H}_j) - f_{\hat{x}_i|t\notin\mathcal{P}_i}(\theta|t \notin \mathcal{P}_i, \mathcal{H}_j) \right\} \times \\ &\left\{ 1 - \mathrm{P}(t \in \mathcal{P}_i|\mathcal{H}_j) \right\} \end{aligned} \tag{8}$$

in which $\mathrm{P}(\cdot)$ denotes the probability of occurrence of the event within parentheses. The above expression results from an application of the conditional probability rule and the fact that the event $(\bar{x}|t \in \mathcal{P}_i)$ is equivalent to $(\hat{x}_i|t \in \mathcal{P}_i)$. As (8) shows, the difference between $f_{\bar{x}}(\theta|\mathcal{H}_j)$ and $f_{\hat{x}_i}(\theta|\mathcal{H}_j)$ is governed by the difference between the conditional PDFs $f_{\bar{x}|t\notin\mathcal{P}_i}(\theta|t \notin \mathcal{P}_i, \mathcal{H}_j)$ and $f_{\hat{x}_i|t\notin\mathcal{P}_i}(\theta|t \notin \mathcal{P}_i, \mathcal{H}_j)$ as well as the probability $\mathrm{P}(t \in \mathcal{P}_i|\mathcal{H}_j)$. If, for instance, the probability $\mathrm{P}(t \in \mathcal{P}_i|\mathcal{H}_j)$ gets close to one, the non-normal PDF $f_{\bar{x}}(\theta|\mathcal{H}_j)$ gets closer to the normal PDF $f_{\hat{x}_i}(\theta|\mathcal{H}_j)$. Depending on the values of i and j, probabilities $\mathrm{P}(t \in$

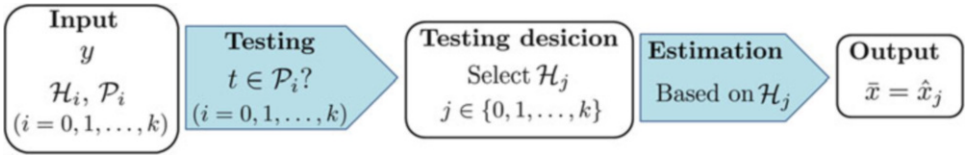

Fig. 1 Schematic illustration of the DIA-method

$\mathcal{P}_i|\mathcal{H}_j)$ $(i, j = 0, 1, \ldots, k)$ can be categorized as

$$\begin{array}{lll} \mathrm{P_{CA}} = \mathrm{P}(t \in \mathcal{P}_0|\mathcal{H}_0) & & \text{Pro. correct acceptance} \\ \mathrm{P_{FA}} = 1 - \mathrm{P_{CA}} & & \text{Pro. false alarm} \\ \mathrm{P_{MD_j}} = \mathrm{P}(t \in \mathcal{P}_0|\mathcal{H}_{j\neq 0}) & & \text{Pro. missed detection} \\ \mathrm{P_{CD_j}} = 1 - \mathrm{P_{MD_j}} & & \text{Pro. correct detection} \\ \mathrm{P_{CI_j}} = \mathrm{P}(t \in \mathcal{P}_{j\neq 0}|\mathcal{H}_{j\neq 0}) & & \text{Pro. correct identification} \\ \mathrm{P_{WI_j}} = \mathrm{P_{CD_j}} - \mathrm{P_{CI_j}} & & \text{Pro. wrong identification} \end{array} \tag{9}$$

where 'Pro.' stands for 'Probability of'. Distinguished by index j, the last four probabilities are different from alternative to alternative. Also note that the last two probabilities become of importance when more than one alternative hypothesis need to be considered. For the single alternative case, say $\mathcal{H}_1$, we have $\mathrm{P_{CI_1}} = \mathrm{P_{CD_1}}$ and $\mathrm{P_{WI_1}} = 0$.

4 Estimation and Testing Strategy

Here, we outline the estimation and testing method as employed in our numerical analysis of the following section. We also remark that our evaluations will be carried out for scalar biases, i.e. $b_i \in \mathbb{R}$, revealing that C_i will take the form of a vector $c_i \in \mathbb{R}^m$.

Estimation To estimate the unknown parameters, use is made of the Best Linear Unbiased Estimation (BLUE) method. As such, $\hat{x}_0$ corresponding with (1) and $\hat{x}_i$ corresponding with (2) are given by

$$\begin{aligned} \hat{x}_0 &= A^+ y = (A^T Q_{yy}^{-1} A)^{-1} A^T Q_{yy}^{-1}\, y \\ \hat{x}_i &= \bar{A}_i^+ y = (\bar{A}_i^T Q_{yy}^{-1} \bar{A}_i)^{-1} \bar{A}_i^T Q_{yy}^{-1}\, y \end{aligned} \tag{10}$$

where the superscript '+' denotes the BLUE-inverse, $\bar{A}_i = P_{c_i}^{\perp} A$ and $P_{c_i}^{\perp} = I_m - c_i(c_i^T Q_{yy}^{-1} c_i)^{-1} c_i^T Q_{yy}^{-1}$. Assuming that the observation vector y is normally distributed, $\hat{x}_0$ and $\hat{x}_i$ in (10), as linear functions of y, have also normal distributions. It can be shown, through the Tienstra transformation (Tienstra 1956; Teunissen 2017b), that all the information in the observation vector y is contained in the two independent vectors $\hat{x}_0$ and t (cf. 3). The estimator $\hat{x}_i$, as a linear function of y, can then be expressed as a linear function of $\hat{x}_0$ and t as

$$\hat{x}_i = \hat{x}_0 - L_i\, t \tag{11}$$

in which $L_i = A^+ c_i (c_{t_i}^T Q_{tt}^{-1} c_{t_i})^{-1} c_{t_i}^T Q_{tt}^{-1}$ with $c_{t_i} = B^T c_i$.

Testing Our testing procedure is specified through defining the regions $\mathcal{P}_0$ and $\mathcal{P}_{i\neq 0}$ (cf. 5) as follows

$$\begin{aligned} \mathcal{P}_0 &= \left\{ t \in \mathbb{R}^r \,\middle|\, \|t\|_{Q_{tt}}^2 \leq k_{\alpha,r} \right\} \\ \mathcal{P}_{i\neq 0} &= \left\{ t \in \mathbb{R}^r / \mathcal{P}_0 \,\middle|\, |w_i| = \max_{j\in\{1,\ldots,k\}} |w_j| \right\}, \quad i = 1, \ldots, k \end{aligned} \tag{12}$$

in which $\|.\|_{Q_{tt}}^2 = (.)^T Q_{tt}^{-1}(.)$, α is the user-defined false alarm probability $\mathrm{P_{FA}}$, $k_{\alpha,r}$ is the α-percentage of the central Chi-square distribution with r degrees of freedom, and w_i is Baarda's test statistic computed as (Baarda 1967; Teunissen 2000)

$$w_i = \frac{c_{t_i}^T Q_{tt}^{-1} t}{\sqrt{c_{t_i}^T Q_{tt}^{-1} c_{t_i}}}; \quad i = 1, \ldots, k \tag{13}$$

5 Numerical Evaluations

In this section, we emphasize the discrepancies between the non-normal PDF of $\bar{x}$ and the normal PDFs of its individual components, i.e. $\hat{x}_i$ $(i = 0, 1, \ldots, k)$. In addition, we investigate situations in which the abnormality of the PDF of $\bar{x}$ gets mitigated. In doing so, we first consider a simple observational model with only a single alternative hypothesis $\mathcal{H}_1$, and then continue with a multiple-hypothesis example in the context of GNSS single point positioning.

5.1 Single-Alternative Case

Suppose that under $\mathcal{H}_0$, the observational model in (1) contains only one unknown parameter $(n = 1)$ with one redundancy $(r = 1)$, i.e. $x \in \mathbb{R}$ and $t \in \mathbb{R}$. We furthermore assume that there is only one single alternative hypothesis, say $\mathcal{H}_1$, against which the null hypothesis $\mathcal{H}_0$ is to be tested. For this binary example, the partitioning of the misclosure space is formed by two regions, $\mathcal{P}_0$ and its complement $\mathcal{P}_0^c$. The DIA-estimator is then constructed by the two estimators $\hat{x}_0$ and $\hat{x}_1$ and the misclosure t as

$$\bar{x} = \hat{x}_0\, p_0(t) + \hat{x}_1(1 - p_0(t)) \tag{14}$$

To compute the PDF of $\bar{x}$, we assume that t, $\hat{x}_0$ and $\hat{x}_1$ are distributed as

$$\begin{array}{ll} t \overset{\mathcal{H}_0}{\sim} \mathcal{N}(0, \sigma_t^2) & , \; t \overset{\mathcal{H}_1}{\sim} \mathcal{N}(\mu_{t_1}, \sigma_t^2) \\ \hat{x}_0 \overset{\mathcal{H}_0}{\sim} \mathcal{N}(0, \sigma_{\hat{x}_0}^2) & , \; \hat{x}_0 \overset{\mathcal{H}_1}{\sim} \mathcal{N}(L_1\mu_{t_1}, \sigma_{\hat{x}_0}^2) \\ \hat{x}_1 \overset{\mathcal{H}_0}{\sim} \mathcal{N}(0, \sigma_{\hat{x}_0}^2 + L_1^2\sigma_t^2) & , \; \hat{x}_1 \overset{\mathcal{H}_1}{\sim} \mathcal{N}(0, \sigma_{\hat{x}_0}^2 + L_1^2\sigma_t^2) \end{array} \tag{15}$$

for some non-zero scalar μ_{t_1}. Note that $\hat{x}_1$ is unbiased both under $\mathcal{H}_0$ and $\mathcal{H}_1$. Under $\mathcal{H}_0$, there is no bias to be considered, and under $\mathcal{H}_1$, $\hat{x}_1$ is obtained based on a model in which the bias b_1 has already been taken into account. With (8), (14) and (15), the difference between the PDF of the DIA-estimator $\bar{x}$ and the normal PDFs of $\hat{x}_0$ and $\hat{x}_1$ is driven by σ_t, $\sigma_{\hat{x}_0}$, L_1, $\mathcal{P}_0$ and the value of μ_{t_1} which comes into play under the alternative hypothesis $\mathcal{H}_1$. In the following, we show how the PDF differences in (8) behave

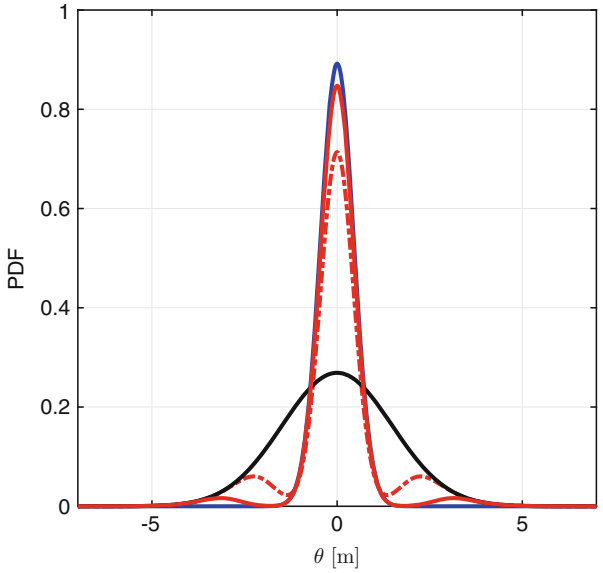

Fig. 2 PDF of the DIA-estimator $\bar{x}$ versus those of $\hat{x}_0$ and $\hat{x}_1$ under $\mathcal{H}_0$ in (14), given $\sigma_t = \sqrt{2}\,\text{m}$, $\sigma_{\hat{x}_0} = \sqrt{0.2}\,\text{m}$ and $L_1 = 1$. *blue*: $f_{\hat{x}_0}(\theta|\mathcal{H}_0)$; *black*: $f_{\hat{x}_1}(\theta|\mathcal{H}_0)$; *red dashed-dotted*: $f_{\bar{x}}(\theta|\mathcal{H}_0)$ for $\text{P}_{\text{FA}} = 0.2$; *red solid*: $f_{\bar{x}}(\theta|\mathcal{H}_0)$ for $\text{P}_{\text{FA}} = 0.05$

as function of some of these parameters under both $\mathcal{H}_0$ and $\mathcal{H}_1$. Note that instead of $\mathcal{P}_0$, we equivalently work with the probability of false alarm $\text{P}_{\text{FA}} = \text{P}(t \in \mathcal{P}_0^c|\mathcal{H}_0)$, which is usually a priori set by the user.

Evaluation Under $\mathcal{H}_0$ Given $\sigma_t = \sqrt{2}\,\text{m}$, $\sigma_{\hat{x}_0} = \sqrt{0.2}\,\text{m}$ and $L_1 = 1$, Fig. 2 shows the normal PDFs of $\hat{x}_0$ (blue) and $\hat{x}_1$ (black) as well as the PDF of $\bar{x}$ (red) under $\mathcal{H}_0$. The DIA-estimator PDF is illustrated for two different values of P_{FA} distinguished by their line style; *dashed-dotted:* $\text{P}_{\text{FA}} = 0.2$, *solid:* $\text{P}_{\text{FA}} = 0.05$. As it can be seen, the PDF of the DIA-estimator does *not* resemble a normal distribution, but in fact a multi-modal distribution. Like the shown two normal PDFs, the red graphs are symmetric w.r.t. the center, which means that the DIA-estimator is unbiased under the null hypothesis, i.e. $\mathsf{E}(\bar{x}|\mathcal{H}_0) = 0$. It is observed that the PDF of the DIA-estimator gets close to the normal PDF of $\hat{x}_0$ as the false alarm probability decreases. It indeed makes sense as decreasing the false alarm probability means that it is getting more likely that the testing procedure leads to the decision to correctly accept the null hypothesis. This in turn will result in the contribution of $\hat{x}_0$ to the construction of $\bar{x}$ getting larger. In the extreme case of $\text{P}_{\text{FA}} = 0$ (no testing), the DIA-estimator PDF becomes identical to the normal PDF of $\hat{x}_0$.

If the data precision Q_{yy} gets scaled by a factor of $\kappa \in \mathbb{R}^+$, then the precision of $\hat{x}_0$, $\hat{x}_1$ and t will also change by exactly the same factor κ (cf. 3, 10). Shown in Fig. 3 are the PDFs of $\hat{x}_0$, $\hat{x}_1$ and $\bar{x}$ under $\mathcal{H}_0$ given $\sigma_t = \kappa \times \sqrt{2}\,\text{m}$, $\sigma_{\hat{x}_0} = \kappa \times \sqrt{0.2}\,\text{m}$, $L_1 = 1$ and $\text{P}_{\text{FA}} = 0.1$. The left panel corresponds with $\kappa = 1$ while the right panel shows the results of $\kappa = 1.5$. In agreement with the normal PDFs of $\hat{x}_0$ and $\hat{x}_1$, the PDF of $\bar{x}$ gets less peaked around the true value when the data in use gets less precise (κ increases).

Evaluation Under $\mathcal{H}_1$ For our analysis under $\mathcal{H}_1$, we need to consider some value for μ_{t_1} as well. With $\mathcal{P}_0$ in (12) and the definition of correct detection probability in (9), the larger the value of b_1 (bias under $\mathcal{H}_1$) and thus μ_{t_1}, the higher is the probability of correct detection. Figure 4 shows, for $\sigma_t = \sqrt{2}\,\text{m}$, $\sigma_{\hat{x}_0} = \sqrt{0.2}\,\text{m}$, $L_1 = 1$ and $\text{P}_{\text{FA}} = 0.1$, the graphs of $f_{\hat{x}_0}(\theta|\mathcal{H}_1)$, $f_{\hat{x}_1}(\theta|\mathcal{H}_1)$ and $f_{\bar{x}}(\theta|\mathcal{H}_1)$. The panels, from left to right, correspond with $\mu_{t_1} = 3\,\text{m}$, $\mu_{t_1} = 4\,\text{m}$ and $\mu_{t_1} = 7\,\text{m}$. Given on top of each panel is the corresponding probability of correct detection. We note that the PDF of the DIA-estimator under $\mathcal{H}_1$ is no longer symmetric around the center, revealing that the DIA-estimator under $\mathcal{H}_1$ is biased, i.e. $\mathsf{E}(\bar{x}|\mathcal{H}_1) \neq 0$. The larger the probability of correct detection gets, the closer the PDF of the DIA-estimator gets towards the normal PDF of $\hat{x}_1$. And ultimately with a correct detection probability larger than 0.99, the PDF $f_{\bar{x}}(\theta|\mathcal{H}_1)$ almost coincides with the PDF $f_{\hat{x}_1}(\theta|\mathcal{H}_1)$ which indeed makes sense as more than 99% of the time, the testing procedure leads to $\mathcal{H}_1$ being selected. We remark that the probability mass of $f_{\bar{x}}(\theta|\mathcal{H}_1)$ becomes more centred around the correct value, or equivalently the DIA-estimator becomes less biased under $\mathcal{H}_1$, for higher correct detection probabilities which can be achieved as a result of larger biases (as shown in Fig. 4), larger false alarm probabilities and/or more precise data.

5.2 Multiple-Alternative Case

In Sect. 5.1, we discussed the properties of the DIA-estimator through some simple examples of binary hypothesis testing applied to a single-unknown, single-redundancy model. With the insight gained from these examples, we now consider the DIA-estimator in the context of a more practical application, i.e. the well-known GNSS single-point positioning (SPP). Assuming that a single GNSS receiver is tracking the pseudorange observations of m satellites on a single frequency, the SPP model under the null hypothesis reads

$$\mathcal{H}_0: \quad \mathsf{E}(y) = [-G \quad e_m] \begin{bmatrix} x \\ dt \end{bmatrix} \quad , \quad \mathsf{D}(y) = \sigma_y^2 I_m \tag{16}$$

with $G \in \mathbb{R}^{m\times 3}$ containing the receiver-satellite unit direction vectors as its rows, $e_m \in \mathbb{R}^m$ containing ones and $I_m \in \mathbb{R}^{m\times m}$ being the identity matrix. There are four unknown parameters to be estimated ($n = 4$); $x \in \mathbb{R}^3$ the receiver

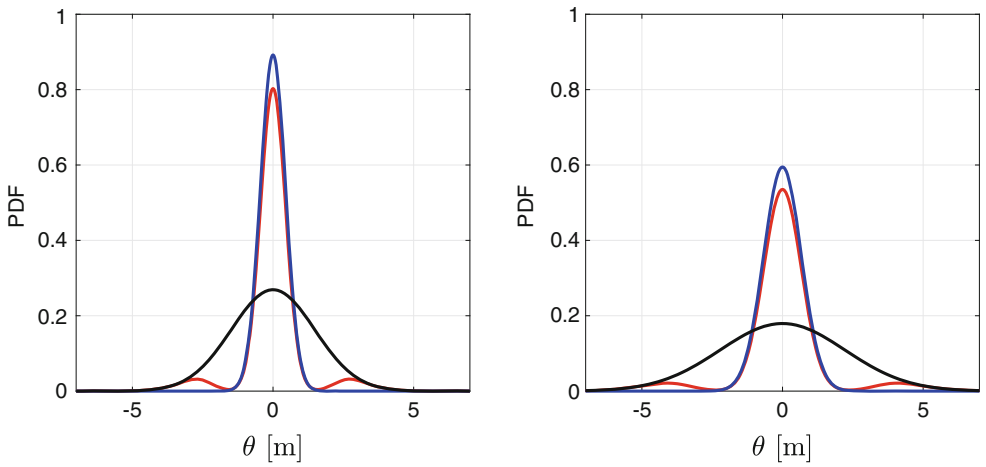

Fig. 3 PDF of the DIA-estimator $\bar{x}$ versus those of $\hat{x}_0$ and $\hat{x}_1$ under $\mathcal{H}_0$ in (14), given $\sigma_t = \kappa \times \sqrt{2}\,\text{m}$, $\sigma_{\hat{x}_0} = \kappa \times \sqrt{0.2}\,\text{m}$, $L_1 = 1$ and $\text{P}_{\text{FA}} = 0.1$ for [left] $\kappa = 1$ and [right] $\kappa = 1.5$. *blue*: $f_{\hat{x}_0}(\theta|\mathcal{H}_0)$; *black*: $f_{\hat{x}_1}(\theta|\mathcal{H}_0)$; *red*: $f_{\bar{x}}(\theta|\mathcal{H}_0)$

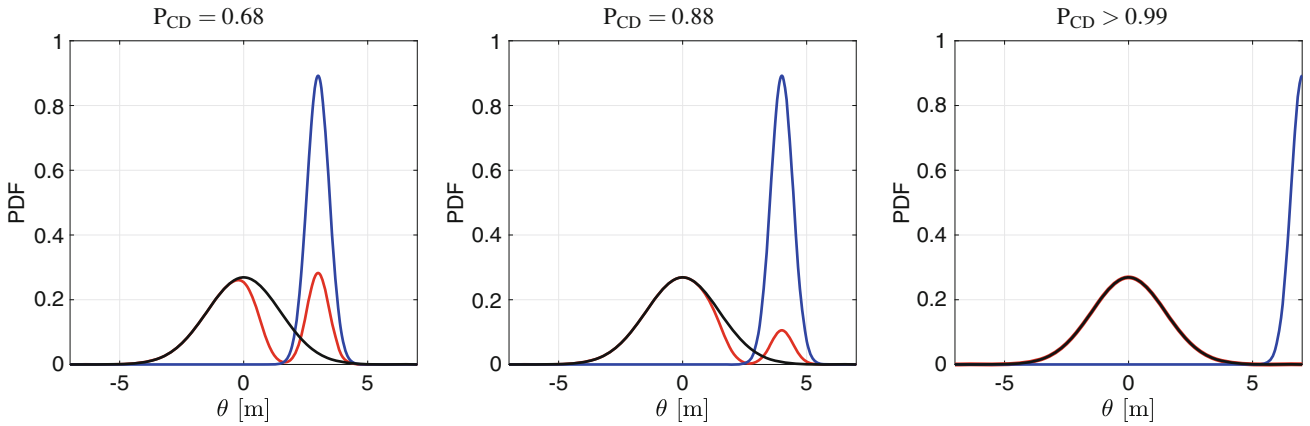

Fig. 4 PDF of the DIA-estimator $\bar{x}$ versus those of $\hat{x}_0$ and $\hat{x}_1$ under $\mathcal{H}_1$ in (14), given $\sigma_t = \sqrt{2}\,\text{m}$, $\sigma_{\hat{x}_0} = \sqrt{0.2}\,\text{m}$, $L_1 = 1$ and $\text{P}_{\text{FA}} = 0.1$ for, [left] $\mu_{t_1} = 3\,\text{m}$, [middle] $\mu_{t_1} = 4\,\text{m}$ and [right] $\mu_{t_1} = 7\,\text{m}$. *blue*: $f_{\hat{x}_0}(\theta|\mathcal{H}_1)$; *black*: $f_{\hat{x}_1}(\theta|\mathcal{H}_1)$; *red*: $f_{\bar{x}}(\theta|\mathcal{H}_1)$. The corresponding correct detection probabilities are given on top of each panel

coordinate components increments and $dt \in \mathbb{R}$ the receiver clock error increment. The redundancy of $\mathcal{H}_0$ is then $r = m - 4$. The dispersion of the observables is characterized through the standard deviation σ_y. At this stage, for the sake of simplicity, we do not consider a satellite elevation-dependent variance matrix.

It is assumed that the alternative hypotheses capture the outliers in individual observations. Thus, with m satellites being available, there are m alternatives $\mathcal{H}_i$ $(i = 1, \ldots, m)$ of the following form

$$\mathcal{H}_i: \quad \mathsf{E}(y) = [-G \quad e_m] \begin{bmatrix} x \\ dt \end{bmatrix} + c_i\, b_i\,, \; \mathsf{D}(y) = \sigma_y^2\, I_m \tag{17}$$

where $c_i \in \mathbb{R}^m$ is a canonical unit vector having one as its i^{th} entry and zero elsewhere, and $b_i \in \mathbb{R}$ is the scalar outlier. Note that the alternative hypotheses in (17) are identifiable provided that $c_{t_i} \nparallel c_{t_j}$ for any $i \neq j$ (Zaminpardaz 2018). For our analysis, we consider the satellite geometry illustrated in Fig. 5, comprising six satellites ($m = 6$).

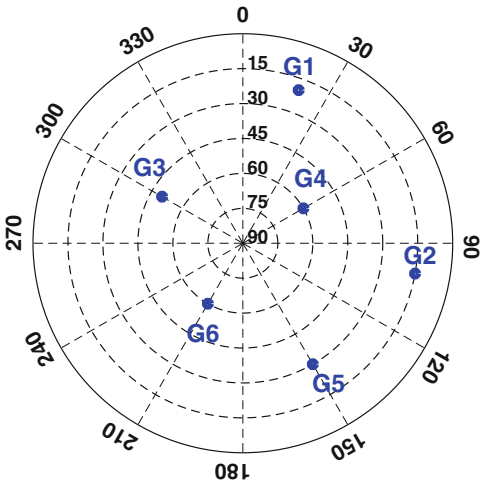

Fig. 5 Skyplot view of satellites. The six blue circles denote the skyplot position of the satellites

Therefore, six alternative hypotheses ($k = m = 6$) of the form of (17) are considered in the DIA procedure, and the

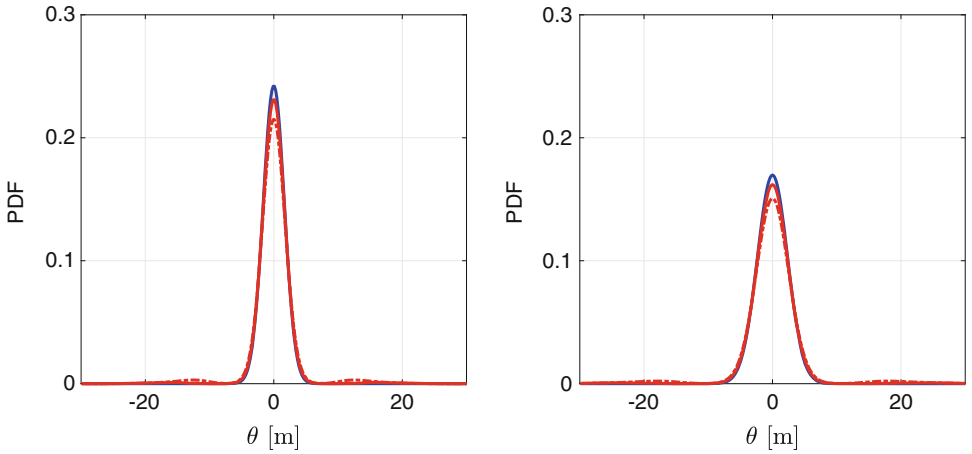

Fig. 6 PDF of the DIA-estimator $\bar{u}$ versus that of $\hat{u}_0$ under $\mathcal{H}_0$. The illustrations are given for the receiver coordinate up component in SPP model in (16) corresponding with the satellite geometry in Fig. 5 for [left] $\sigma_y = 0.7$ m and [right] $\sigma_y = 1$ m. *blue*: $f_{\hat{u}_0}(\theta|\mathcal{H}_0)$; *red dashed-dotted*: $f_{\bar{u}}(\theta|\mathcal{H}_0)$ for $\mathrm{P_{FA}} = 0.3$; *red solid*: $f_{\bar{u}}(\theta|\mathcal{H}_0)$ for $\mathrm{P_{FA}} = 0.1$

redundancy under the null hypothesis is $r = 2$ ($t \in \mathbb{R}^2$). We also remark that for this satellite geometry, all the six alternatives are identifiable. Our illustrations will be shown for receiver coordinate up component, denoted by u, under $\mathcal{H}_0$, $\mathcal{H}_1$ (outlier in G1 observation) and $\mathcal{H}_4$ (outlier in G4 observation). However, we note that our conclusions will be valid for any unknown parameter in (16). Without loss of generality, we also assume that the true value of the up component is zero.

Evaluation Under $\mathcal{H}_0$ In Fig. 6, the PDFs of $\hat{u}_0$ and $\bar{u}$ are depicted in, respectively, blue and red color. The left panel shows the results corresponding with $\sigma_y = 0.7$ m while the right one shows the results corresponding with $\sigma_y = 1$ m. In each panel two red graphs are illustrated; *dashed-dotted*: $\mathrm{P_{FA}} = 0.3$, *solid*: $\mathrm{P_{FA}} = 0.1$. Again the symmetry of the DIA-estimator PDF around the true value indicates the unbiasedness of the DIA-estimator under the null hypothesis. In addition, the peakedness of the DIA-estimator PDF, like the PDF of $\hat{u}_0$, around the true value decreases when the data precision gets poorer (σ_y increases). Similar to the single-alternative example, we expect that the difference between the red and blue graphs will diminish if the false alarm probability decreases. This is indeed corroborated by comparing the red dashed-dotted graphs with the red solid ones in Fig. 6.

Evaluation Under $\mathcal{H}_1$ and $\mathcal{H}_4$ For our analysis under alternative hypotheses, we, as example, take the two alternatives $\mathcal{H}_1$ and $\mathcal{H}_4$. Assuming $\sigma_y = 1$ m and $\mathrm{P_{FA}} = 0.1$, Fig. 7 shows the PDFs of $\hat{u}_0$, $\hat{u}_i$ and $\bar{u}$ under $\mathcal{H}_i$. The top panels are given for $i = 1$ while the bottom panels are obtained for $i = 4$. The values for b_i under the mentioned two alternatives are, from left to right, set to $b_i = 3,\ 7$ and 15m. Here, because of having more than one single alternative, in addition to the correct detection probability, we also compute the correct identification probability, both of which are shown on top of each panel.

The significant departure between the red graph and the other two normal curves in each panel is an indicator of how misleading the post-DIA quality assessments would be if one neglects the conditioning on testing outcome. For example, let us assume that, for the case of lower-right panel, $\mathcal{H}_4$ is selected through the DIA procedure. As shown in Fig. 7, the PDF of $\hat{u}_4$ has larger probability mass around the true value than that of $\bar{u}$. Therefore, assessments on the basis of $f_{\hat{u}_4}(\theta|\mathcal{H}_4)$, rather than $f_{\bar{u}}(\theta|\mathcal{H}_4)$, would lead to optimistic/misleading quality descriptions (precision, accuracy, integrity, etc.). As the bias value b_i increases, both the correct detection and identification probabilities increase as well, resulting in less discrepancies between $f_{\hat{u}_i}(\theta|\mathcal{H}_i)$ and $f_{\bar{u}}(\theta|\mathcal{H}_i)$. Note, however, that the difference between the red graphs and the corresponding black ones becomes small only for large *correct identification* probabilities, and not necessarily for large *correct detection* probabilities. For example, for the case where bias under $\mathcal{H}_1$ is $b_1 = 7$ m (upper-middle panel), despite having a large correct detection probability of $\mathrm{P_{CD_1}} = 0.94$, there is a big difference between the red and black curve as the correct identification probability is only $\mathrm{P_{CI_1}} = 0.60$.

6 Summary and Concluding Remarks

There is a close link between estimation and testing in any quality control procedure. By highlighting this link and its consequences, we revealed its impact on the quality evaluations usually performed and elaborated on the circumstances under which negligence of this link may still be considered acceptable. In doing so, we provided a comparative study of the probabilistic properties of the actual DIA outcome $\bar{x}$ derived from the characteristics of both estimation and testing, and the individual estimators $\hat{x}_i$ corresponding with the hypotheses at hand $\mathcal{H}_i$ ($i = 0, 1, \ldots, k$) neglecting the uncertainty of the testing decision process. Our analyses were conducted assuming that the observations are normally distributed and that the underlying models are linear.

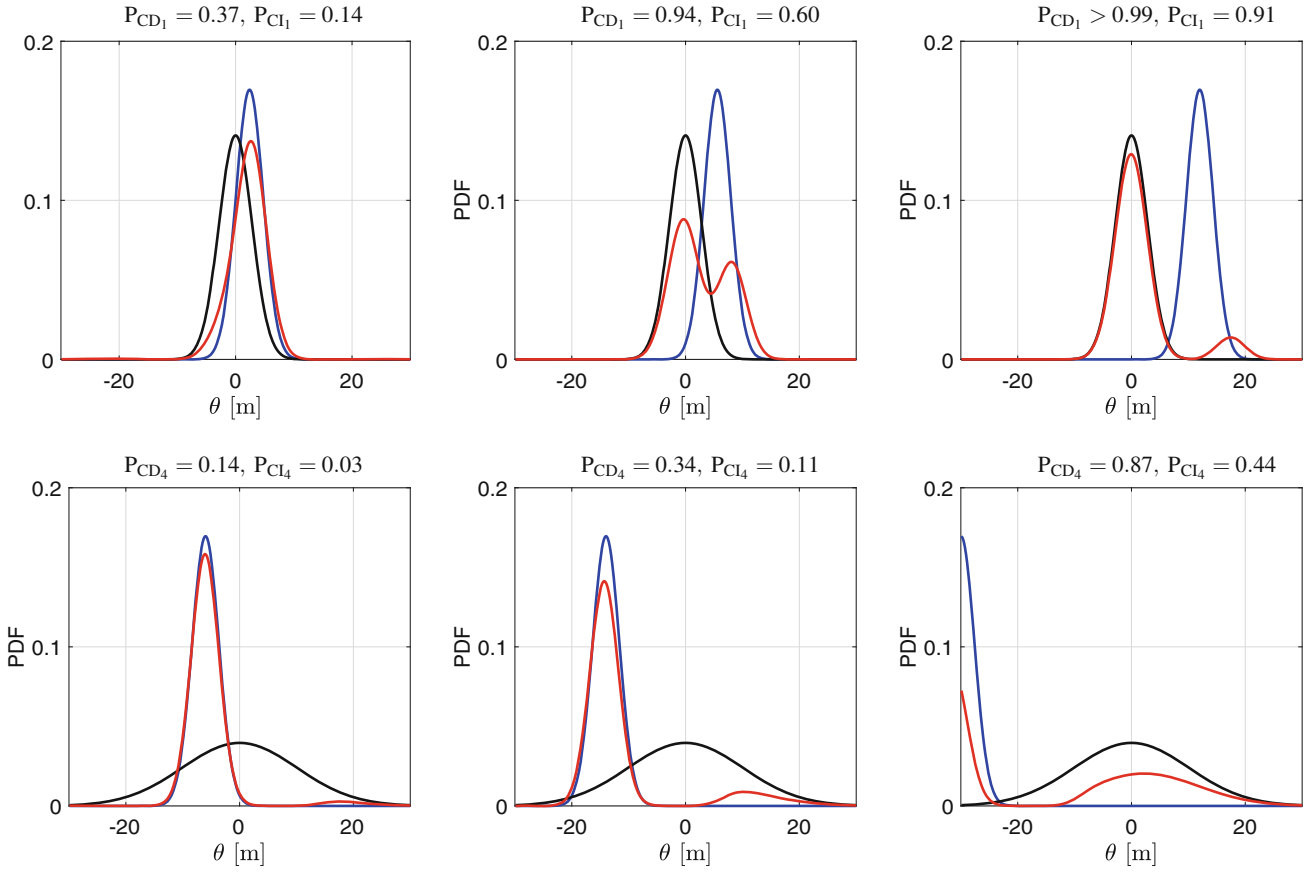

Fig. 7 PDF of the DIA-estimator $\bar{u}$ versus those of $\hat{u}_0$ and $\hat{u}_i$ under $\mathcal{H}_i$ in (17) for [top] $i = 1$ and [bottom] $i = 4$. The illustrations are given for $\sigma_y = 1$ m and for [left] $b_i = 3$ m, [middle] $b_i = 7$ m and [right] $b_i = 15$ m. *blue*: $f_{\hat{u}_0}(\theta|\mathcal{H}_i)$; *black*: $f_{\hat{u}_i}(\theta|\mathcal{H}_i)$; *red*: $f_{\bar{u}}(\theta|\mathcal{H}_i)$. The corresponding correct detection and identification probabilities are given on top of each panel

We started with simple examples of single alternative hypothesis where a single-unknown, single-redundancy model was considered. The DIA-estimator was then constructed by $\hat{x}_0$, $\hat{x}_1$ and t. It was demonstrated that the distribution of the DIA-estimator, unlike its individual constructing components, is not normal, but multi modal. However, the non-normal PDF of $\bar{x}|\mathcal{H}_0$ ($\bar{x}|\mathcal{H}_1$) will approach the normal distribution of $\hat{x}_0|\mathcal{H}_0$ ($\hat{x}_1|\mathcal{H}_1$) if P_{FA} ($P_{MD} = 1 - P_{CD}$) decreases. The impact of the data precision on the DIA-estimator PDF was also illustrated. For example, under $\mathcal{H}_0$, the more precise the observations are, the more peacked the DIA-estimator PDF gets around the true value. It was also shown that while $\bar{x}$ is unbiased under $\mathcal{H}_0$, it is biased under $\mathcal{H}_1$. The bias of $\bar{x}|\mathcal{H}_1$ gets, however, smaller when the correct detection probability gets larger as more probability mass of $f_{\bar{x}}(\theta|\mathcal{H}_1)$ becomes centred around the true value.

Having investigated the single-alternative case, we then applied the DIA-method to the satellite-based single point positioning model where multiple alternative hypotheses, describing outliers in individual observations, were considered. For our illustrations, we showed the results corresponding with the receiver coordinate up component u. We however remark that the following conclusions are valid for any other unknown parameter and linear model. Similar to the single-alternative example, it was shown that the PDF of the DIA-estimator $\bar{u}$ cannot be characterized by a normal distribution. Depending on the underlying settings, there could be significant departures between the PDF of the DIA-estimator and that of the estimator associated with the identified hypothesis. It was highlighted that if the uncertainty of the statistical testing is not taken into account, then one may end up with a too optimistic quality description of the final estimator. Nevertheless, depending on the requirements of the application at hand, the DIA-estimator PDF may be well approximated by $\hat{u}_0|\mathcal{H}_0$ under $\mathcal{H}_0$ and by $\hat{u}_i|\mathcal{H}_i$ under $\mathcal{H}_i$ for, respectively, small P_{FA} and large P_{CI_i}. It is therefore important that one always properly evaluates identification probabilities, as a large probability of correct detection not necessarily implies a large correct identification probability (Teunissen 2017b).

References

Baarda W (1967) Statistical concepts in geodesy. Netherlands Geodetic Commission, Publ. on geodesy, New series 2(4)

Baarda W (1968) A testing procedure for use in geodetic networks. Netherlands Geodetic Commission, Publ. on geodesy, New Series 2(5)

DGCC (1982) The Delft Approach for the Design and Computation of Geodetic Networks. In: "Forty Years of Thought" Anniversary edition on the occasion of the 65th birthday of Prof W Baarda, vol 2, pp 202–274. By staff of the Delft Geodetic Computing Centre (DGCC)

Khodabandeh A, Teunissen PJG (2016) Single-epoch GNSS array integrity: an analytical study. In: Sneeuw N, Novák P, Crespi M, Sansò F (eds) VIII Hotine-Marussi symposium on mathematical geodesy: proceedings of the symposium in Rome, 17–21 June, 2013. Springer International Publishing, Cham, pp 263–272

Klein I, MatsuokaMatheus MT, Guzatto MP, Nievinski FG, Veronez MR, Rofatto VF (2018) A new relationship between the quality criteria for geodetic networks. J Geodesy 1–16. https://doi.org/10.1007/s00190-018-1181-8

Perfetti N (2006) Detection of station coordinate discontinuities within the Italian GPS fiducial network. J Geodesy 80(7):381–396

Salzmann M (1995) Real-time adaptation for model errors in dynamic systems. Bull Geodesique 69:81–91 (1995)

Teunissen PJG (1990) An integrity and quality control procedure for use in multi-sensor integration. In: Proc of ION GPS-1990. ION, pp 513–522

Teunissen PJG (2000) Testing theory: an introduction, Series on mathematical geodesy and positioning. Delft University Press, Delft

Teunissen PJG (2017a) Batch and recursive model validation. In: Teunissen PJG, Montenbruck O (eds) Springer handbook of global navigation satellite systems, chapter 24, pp. 727–757

Teunissen PJG (2017b) Distributional theory for the DIA method. J Geodesy 1–22. https://doi.org/10.1007/s00190-017-1045-7

Teunissen PJG, Imparato D, Tiberius CCJM (2017) Does RAIM with correct exclusion produce unbiased positions? Sensors 17(7):1508

Tiberius CCJM (1998) Recursive data processing for kinematic GPS surveying. Netherlands Geodetic Commission, Publ. on Geodesy, New series (45)

Tienstra J (1956) Theory of the adjustment of normally distributed observation. Argus, Amsterdam

Zaminpardaz S, Teunissen PJG (2018) DIA-datasnooping and identifiability. J Geodesy 1–17 (2018). https://doi.org/10.1007/s00190-018-1141-3

Zaminpardaz S, Teunissen PJG, Nadarajah N, Khodabandeh A (2015) GNSS array-based ionospheric spatial gradient monitoring: precision and integrity analysis. In: Proceedings of the ION Pacific PNT meeting. ION, pp 799–814